Computers and Fluids 134–135 (2016) 31–40

Contents lists available at ScienceDirect

Computers and Fluids

journal homepage: www.elsevier.com/locate/compfluid

Dynamics of a nonspherical capsule in general flow

Huilin Ye[a], Haibo Huang[a,*], Yi Sui[b], Xi-Yun Lu[a]

[a] Department of Modern Mechanics, University of Science and Technology of China, Hefei, Anhui 230026, China
[b] School of Engineering and Materials Science, Queen Mary University of London, London E1 4NS, United Kingdom

ARTICLE INFO

Article history:
Received 25 January 2016
Revised 8 May 2016
Accepted 12 May 2016
Available online 14 May 2016

Keywords:
Deformable particle
Capsule dynamics
Lattice Boltzmann
General flow
Fluid structure interaction

ABSTRACT

The dynamics of a capsule in general flows is studied analytically and numerically. The capsule is modeled as a liquid-filled drop enclosed by a membrane. We adapted the Keller-Skalak (KS) theory and Skotheim-Secomb model to the case of general flow, the governing equations are derived. It is found that when viscosity ratio $\lambda = 1$, the capsule dynamics in general flows is controlled by two dimensionless parameters, the ratio of vorticity to strain rate of the flow and the ratio of the elastic force to fluid stress. In the literature, the transition between swinging (SW) and tumbling (TU) is always one way (TU to SW). As far as we know, it is the first time that the TU-SW-TU transition has been identified, i.e., the transition may also transfer from SW to TU after the transition (TU to SW) occurs under some circumstances. The possible mechanism is that the rotation of the flow suppresses the deformation along the vorticity direction of the capsule. The shape dynamics of a capsule is studied in detail and the rheology of dilute capsule suspension is also investigated briefly.

1. Introduction

Soft biological particles, such as vesicles, cells and capsules, have drawn much attention for many years and there are many theoretical, numerical, and experimental studies [1–8]. Detailed studies of a single particle are critical for understanding the rheology of bio-fluids. However, till today even behaviors of one single particle is not fully understood. A complete theoretical study in this topic is not easy. For example, the shape of the particle is not given *a priori* and continuously deforming. The shape evolution of the particle is determined by the dynamic balance between the interfacial forces and fluid stresses. To simplify the theoretical analysis, some studies [9,10] constrained the number of degrees of freedom and others [11,12] applied asymptotic analyses to investigate the dynamics. Due to the difficulties in theoretical study, there are many experimental [5,13] or numerical studies [2,14–17].

Here, we define capsule as a kind of unbreakable, hermetic membrane which is chemically or physically cross-linked [18]. The membrane provides the resistance to shear and to change of volume. It has been shown that there is a steady tank-treading motion in simple shear flow when the capsule is initially spherical [14]. If the capsule is not initially spherical, a transition from tank-treading to tumbling may occur through reducing shear rate or increasing viscosity ratio λ [10,15]. The swinging mode, which lies between tank-treading and tumbling, has been experimentally detected for red blood cells (RBCs) [1,9]. In this mode, the shape deformation is periodic and the inclination oscillates around a mean angle with respect to the direction of the flow. The swinging mode has also been found for capsule [15]. Due to the lacking of bending effect in capsule, the wrinkles would occur because of the compressive stress in the membrane that is imposed by the flow [19–21].

Unlike capsules, vesicles exhibit a strong resistance to changes of volume, total surface area, and bending. Vesicles are not sensitive to strain. Hence, they can not show shear elasticity [15]. There are numerous theoretical and experimental studies on vesicles. In the KS theory [10], the particle is supposed to be a shape-fixed ellipsoid, which is enclosed by an inextensible membrane. And transition from tank-treading to tumbling mode is investigated. Fischer [22] introduced a shape memory model for the RBCs, in which, the rim of a red blood cell is always consisted of the same part of the membrane after relaxation from deformation. A regime of intermittent dynamics, characterized by several swinging cycles interrupt by a tumbling regularly near the transition from tank-treading to tumbling, was first observed by experiment [1]. Benefiting from the shape memory model [22], Abkarian et al. [1] and Skotheim et al. [9] introduced the energy barrier for the membrane based on the KS theory, and the model is able to predict the existence of the intermittent motion.

However, this intermittent motion is unable to be obtained in numerical simulations [3,16,23,24]. Considering the shape parameter, Noguchi [25,26] predicted the synchronized rotation of phase

* Corresponding author.
E-mail address: huanghb@ustc.edu.cn (H. Huang).

http://dx.doi.org/10.1016/j.compfluid.2016.05.011
0045-7930/

angle and inclination angle with integer ratios of the frequencies, which is different from the intermittent motion predicted by [9]. Vlahovska et al. [27] concluded that the intermittent behavior in [9] is a result of the shape-fixed assumption in the reduced models, in which only small-deformation is considered. They also pointed out that the intermittent behavior would be suppressed if there is a deformation along the vorticity direction. However, in the simple shear flow, the deformation along the vorticity direction is inevitable. Hence, the intermittent motion is difficult to be observed.

Although Abkarian et al. [1] observed the intermittent behavior, the mechanism is not fully understood. Now days, numerical simulations become an important tool to study the intermittent dynamics. Cordasco et al. [28] and Peng et al. [29] showed that there is a large deformation along the vorticity direction during the TU-SW transition. More recently, Cordasco and Bagchi [4] present the computational evidence for the intermittent motion, which is characterized by an irregular sequence of TU interrupted by an SW, or vice versa, and synchronized motion with the cell rotation and membrane rotation with integer ratio of the rotational frequencies. The membrane in-plane elastic energy is introduced to explain these dynamics observed in the simulations [4].

However, the intermittent behavior research mentioned above are all based on the dynamics of vesicle and RBCs, in which the bending effects cannot be ignored [30]. In present work, we focus on capsule's intermittent dynamics without bending stiffness. Benefiting from the conclusion that the intermittent behavior would be suppressed by deformation along the vorticity direction [27], we introduce an important dimensionless parameter, the ratio of the vorticity to the strain rate [31]. The elastic energy form in the model of Skotheim and Secomb [9] is based on the shape memory model, which is derived from experiment data. Here, an concrete energy form derived from the nonlinear membrane constitutive model is used in both our theoretical analysis and numerical simulations. It is expected to yield a better theoretical and numerical comparison. The capsule's membrane is assumed to follow the neo-Hookean (NH) law. It is found that the transition from TU to SW is no longer one way, i.e., an initial tumbling capsule may return to TU state after the TU-SW transition rather than eventually reach a stable swinging state.

The present work is intended to provide a better understanding of the behavior of an initially nonspherical capsule in general flow. In this work, the dynamics of a nonspherical capsule is studied both analytically and numerically. First, the analytical calculation help us to determine dimensionless parameters. Because a capsule in general flow is different from the capsule in elongational and simple shear flow, the dimensionless parameters for the two flows may be not identical. Second, although there are some assumptions in the theoretical analysis, the approximate phase diagram for the motion of the capsule can be obtained through the theoretical analysis. The approximate phase diagram is helpful for parameter chosen in our numerical simulations.

In Section 2, the theoretical model and numerical method are introduced briefly. Next, in Section 3, through numerical simulations, accurate phase diagram can be obtained. Our results for the mode transition and shape dynamics are discussed and compared with the theoretical predictions. Also, the rheology of dilute suspension is investigated briefly. Finally, conclusions are presented in Section 4.

2. Methods

2.1. Theoretical model

In this section, our derivation follows the theoretical frame in [9,10]. The equations for the motion of capsules based on Jeffery's theory [32] have been derived by Keller and Skalak [10] analytically. They also improved the results of Roscoe [33], in which the inclination angle of the particle is assumed constant. Here, more general flows beyond simple shear flow are considered in our derivation, and the flow is still a plane flow. The undisturbed flow with a space-fixed frame shown in Fig. 1 is denoted by $\widehat{u}_i^0$, the velocity gradient is

$$\delta_i u_j^0 = s_{ij} - \epsilon_{ijk}\omega_k, \tag{1}$$

where s_{ij} is the symmetric strain tensor, ω_k is the vorticity vector. $s = \sqrt{tr(s_{ij}^2)/2}$ and $\omega = |\omega_k|$ are the strain rate and the vorticity, respectively. Here an important dimensionless parameter is defined as

$$\Xi \equiv \omega/s, \tag{2}$$

which refers to the ratio of vorticity to strain rate. Then the velocity field of fluid is obtained as

$$u_1^0 = (s+\omega)\widehat{x}_2,\ u_2^0 = (s-\omega)\widehat{x}_1,\ u_3^0 = 0. \tag{3}$$

Due to the moment balance of the capsule, the rate of change of the inclination angle θ is obtained as [10]

$$\partial_t\theta = -\omega - \frac{2a_1a_2}{a_1^2+a_2^2}\partial_t\phi + s\frac{a_1^2-a_2^2}{a_1^2+a_2^2}cos2\theta, \tag{4}$$

where a_1 and a_2 are semi-major axis and semi-minor axis in the shear plane, respectively. If the velocity and stress field shown in Appendix A are known, the internal dissipation D and the rate of work W_p done by the external fluid on the ellipsoid can be derived (refer to [10] for more details):

$$D = V\mu' f_1(\partial_t\phi)^2, \tag{5}$$

$$W_p = V\mu(f_2(\partial_t\phi)^2 + 2sf_3\partial_t\phi cos2\theta), \tag{6}$$

the parameters are defined in Appendix A and V is the volume of the capsule. The work done by external fluid on the capsule is not only consumed by the internal dissipation, but also transferred to the elastic energy stored in the membrane [1,9]. Suppose that the membrane follows the neo-Hookean law, which has the energy form [34]

$$W^{NH} = \frac{1}{6}E\left(I_1 - 1 + \frac{1}{I_2+1}\right), \tag{7}$$

where E is the Young's modulus, and $I_1 = \lambda_1^2+\lambda_2^2-2$, $I_2 = (\lambda_1\lambda_2)^2-1$ are the first and second strain invariants, respectively. λ_1 and λ_2 are the principle strains. Here the elastic energy form is

$$W^{NH} = \frac{2}{3}z_1^2 Esin^2\phi, \tag{8}$$

and the detailed derivation is shown in Appendix B.

The energy balance of the capsule is

$$W_p = D + \partial_t \oint_{S_c} W^{NH}, \tag{9}$$

this yields

$$V\mu(f_2(\partial_t\phi)^2 + 2sf_3\partial_t\phi cos2\theta = V\mu' f_1(\partial_t\phi)^2 + \frac{2}{3}ES_c z_1^2 sin2\phi\partial_t\phi, \tag{10}$$

where S_c is the surface area of the capsule.

Combining Eqs. (4) and (10) and scaling time with $t = T/2s$, it yields the dimensionless evolution equations for phase angle ϕ and

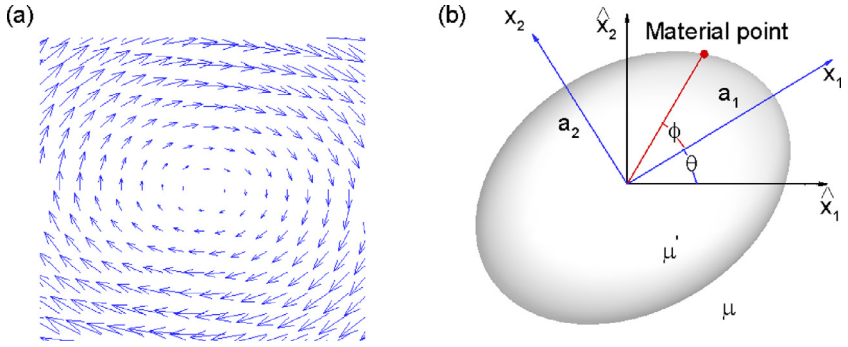

Fig. 1. The schematic diagram of the model. (a) the velocity field of the flow with $\Xi = 4$, (b) the membrane model of an ellipsoidal capsule in general flow.

Table 1
Comparison of parameters.

	Type	Excess area	Viscosity ratio	Membrane property	Ratio of vorticity to stain rate
Ref. [36]	Vesicle	Δ	λ	κ	$\frac{\omega}{s}$
Ref. [37]	Vesicle	Δ	λ	κ	NA
present	Capsule	Δ	λ	E_s	$\Xi = \frac{\omega}{s}$

inclination angle θ,

$$\partial_T \phi = h_1(\Lambda sin2\phi + cos2\theta),$$
$$\partial_T \theta = -\frac{1}{2}\Xi - h_2\partial_T\phi + h_3 cos2\theta, \tag{11}$$

where $h_1 = -\frac{f_3}{f_2 - \lambda f_1}, h_2 = \frac{2a_1a_2}{a_1^2+a_2^2}, h_3 = \frac{a_1^2-a_2^2}{2(a_1^2+a_2^2)}$. Suppose R_0 is an equivalent spherical radius for capsule volume V, i.e., $V = \frac{4}{3}\pi R_0^3$ and we define $S_c = (4\pi + \Delta)R_0^2$, another important dimensionless parameter Λ is

$$\Lambda \equiv -\frac{(4\pi + \Delta)Ez_1^2}{4\pi R_0 \mu f_3 s}. \tag{12}$$

Now the equations for the evolutions of phase angle ϕ and inclination angle θ are derived. They are totally characterized by three dimensionless parameters λ, Ξ and Λ under the assumption that the capsule preserves an undeformed shape. In present work, the main task is to study the influence of vorticity on the dynamics of the capsule. Because the viscosity ratio effects have been studied extensively [10,23,26,35], the viscosity ratio λ is set to be unity in our study. We focus on the effects of Ξ and Λ.

Here we would like to perform a comparison for key parameters in the literature. Lebedev et. [36] and Kaoui et al. [37] claimed that the dynamics of vesicle depends on two and three dimensionless parameters, respectively. Actually the nondimensional parameters are consistent in the two works. The key parameters in [36,37] and the present work is listed in Table 1. The membrane property in the table means bending rigidity or shear elasticity. Lebedev et al. [36] considered the rotational effect while Kaoui et al.[37] did not. Two nondimensional parameters in Lebedev et al. [36] were derived from the four parameters listed in the table through theoretical analysis. However, Kaoui et al. [37] using the three parameters listed in the table directly and "it may be useful for any future attempts to analyze experimental data" [37].

It is also noticed that the two works [36,37] both investigated vesicles instead of capsules. They payed attention to the bending effect and the membrane is treated as incompressible in their vesicle model. However, in our capsule model, the bending effect is not considered, and the membrane is not treated as incompressible, which results in shear elasticity.

In our study, three nondimensional parameters λ, Ξ, and Λ are derived from the four parameters listed in Table 1 through theoretical analysis, which is similar to the procedure in [36]. Three parameters may be the minimum requirement to describe properly the dynamics of a capsule.

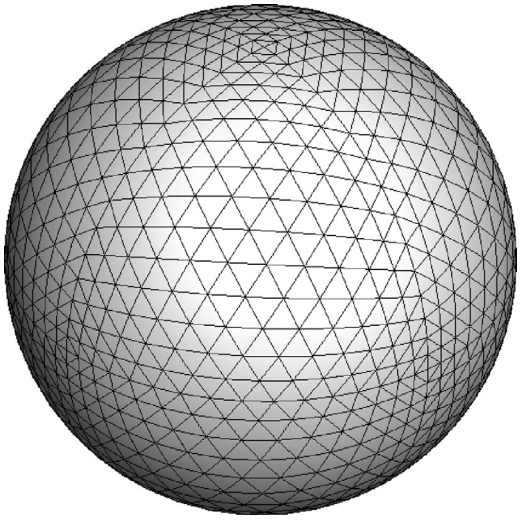

Fig. 2. Discretization of a sphere.

2.2. Numerical method

2.2.1. Finite element membrane model

In our study, the membrane dynamics is numerically solved by finite element method, in which the neo-Hookean constitutive law (7) is adopted. The 3D capsule membrane is discretized into flat triangular elements. To discretize the unstressed interface, each triangular face of a regular octahedron is subdivided into 4^n triangular elements. These elements are then projected radically onto a sphere. The geometry of each element is described by its three vertices. The discretization of a sphere surface is shown in Fig. 2. For oblate spheroid, it is necessary to make the coordinates multiply by the aspect ratio of the oblate spheroid.

First, the problem is reduced to a 2D(planar) deformation by transforming the undeformed and deformed surface elements to a common plane using rigid-body rotations, the detailed method is given in [34]. Here gives the in-plane displacements **v** of the vertices and the displacement gradient tensor **D**. Then the in-plane

principal strains are:

$$\lambda_i^2 = \frac{1}{2}[G_{11} + G_{22} \pm \sqrt{(G_{11} - G_{22})^2 + 4G_{12}^2}], i = 1, 2, \tag{13}$$

where $\mathbf{G} = \mathbf{D}^T\mathbf{D}$. The elastic forces acting on the three vertices of a triangular element are obtained from the strain energy function W^{NH} using the principal of virtual work as

$$\mathbf{f}(\mathbf{x}', t) = -\frac{\partial W^{NH}}{\partial \mathbf{x}'}. \tag{14}$$

Then, the in-plane force $\mathbf{f}^p$ can be obtained as

$$\mathbf{f}^p = \frac{\partial W^{NH}}{\partial \lambda_1}\frac{\partial \lambda_1}{\partial \mathbf{v}} + \frac{\partial W^{NH}}{\partial \lambda_2}\frac{\partial \lambda_2}{\partial \mathbf{v}}. \tag{15}$$

Because each node of the discrete membrane belongs to more than one element, the resultant force on a node is the sum of the forces exerted by the surrounding elements directly attached to the node. So far, the calculated force is the fluid force acting on the capsule membrane. Its equal and opposite counterpart is the force acting on the fluid. It is distributed to the surrounding fluid by the immersed boundary method which will be discussed below.

2.2.2. Multi-block lattice Boltzmann method

The general flow is solved by Lattice Boltzmann method (LBM), which is an efficient solver for the Navier–Stokes (NS) equations with a low Reynolds number. Here, the D3Q19 model is used and the discrete lattice Boltzmann equation (LBE) reads

$$f_i(\mathbf{x} + \mathbf{e}_i\Delta t, t + \Delta t) = f_i(\mathbf{x}, t) - \frac{1}{\tau}(f_i(\mathbf{x}, t) - f_i^{eq}(\mathbf{x}, t)), \tag{16}$$

where $f_i(\mathbf{x}, t)$ is the distribution function for particles with velocity $\mathbf{e}_i$ at position $\mathbf{x}$ and time t, Δt is the lattice time interval, $f_i^{eq}(\mathbf{x}, t)$ is the equilibrium distribution function and τ is the non-dimensional relaxation time.

In the D3Q19 model, the fluid particles have the possible discrete velocities stated as follows [34,38]:

$$[\mathbf{e}_0, \mathbf{e}_1, \mathbf{e}_2, \mathbf{e}_3, \mathbf{e}_4, \mathbf{e}_5, \mathbf{e}_6, \mathbf{e}_7, \mathbf{e}_8, \mathbf{e}_9, \mathbf{e}_{10}, \mathbf{e}_{11}, \mathbf{e}_{12}, \mathbf{e}_{13}, \mathbf{e}_{14}, \mathbf{e}_{15}, \mathbf{e}_{16}, \mathbf{e}_{17}, \mathbf{e}_{18}] =$$
$$\begin{bmatrix} 0 & 1 & -1 & 0 & 0 & 0 & 0 & 1 & 1 & -1 & -1 & 1 & -1 & 1 & -1 & 0 & 0 & 0 & 0 \\ 0 & 0 & 0 & 1 & -1 & 0 & 0 & 1 & -1 & 1 & -1 & 0 & 0 & 0 & 0 & 1 & 1 & -1 & -1 \\ 0 & 0 & 0 & 0 & 0 & 1 & -1 & 0 & 0 & 0 & 0 & 1 & 1 & -1 & -1 & 1 & -1 & 1 & -1 \end{bmatrix}. \tag{17}$$

The equilibrium distribution function $f_i^{eq}(\mathbf{x}, t)$ can be calculated as:

$$f_i^{eq}(\mathbf{x}, t) = \omega_i\rho\left[1 + \frac{\mathbf{e}_i \cdot \mathbf{u}}{c_s^2} + \frac{(\mathbf{e}_i \cdot \mathbf{u})^2}{2c_s^4} - \frac{(\mathbf{u})^2}{2c_s^2}\right], \tag{18}$$

where the weighting coefficients $\omega_i = 1/3 (i = 0)$, $\omega_i = 1/18 (i = 1 - 6)$, $\omega_i = 1/36 (i = 7 - 18)$. The term c_s represents the sound speed which equals $\Delta x/(\sqrt{3}\Delta t)$.

The relaxation time is related to the kinematic viscosity ν by

$$\nu = \left(\tau - \frac{1}{2}\right)c_s^2\Delta t. \tag{19}$$

Once the particle density distribution is known, the fluid density and momentum are calculated as

$$\rho = \sum_i f_i, \qquad \rho\mathbf{u} = \sum_i f_i\mathbf{e}_i. \tag{20}$$

Here the multi-block lattice Boltzmann method proposed by Yu and Girimaji [39] is employed. We consider a two-block system, the computational domain is divided into two blocks which are connected through the interface. The lattice space ratio between coarse and fine grids equals two. The capsule is immersed in the fine mesh block. On the interface between the two blocks, the exchange of variables follows a certain relation so that the mass and momentum are conserved and the stress is continuous across the interface. Detailed method is explained in [34].

2.2.3. Immersed boundary method

In our study, the immersed boundary method is adopted to couple the finite element model with the lattice Boltzmann method, in which a force density is distributed to the Cartesian mesh in the vicinity of the moving boundary in order to account for the effect of the boundary. In the follows, $\mathbf{x}$ represents a point in the Eulerian coordinates, which is used to solve the fluid flow. $\mathbf{s}$ represents a boundary node of the capsule in a Lagrangian coordinates, which is used to solve the deformation of the membrane. In the Eulerian coordinates, the position of a Lagrangian node $\mathbf{s}$ on the capsule membrane is $\mathbf{X}(\mathbf{s}, t)$, which has three components $\mathbf{X} = (X, Y, Z)$.

In order to satisfy the no-slip boundary condition, the flexible membrane should move with the same velocity as the fluid around it. That is

$$\frac{\partial \mathbf{X}(\mathbf{s}, t)}{\partial t} = \mathbf{u}(\mathbf{X}(\mathbf{s}, t)). \tag{21}$$

This condition will cause the capsule to deform. The membrane force density $\mathbf{F}(\mathbf{s}, t)$, which is induced by capsule deformation, is obtained by the finite element membrane model discussed in Section 2.2.1, and is distributed to the fluid mesh points near it by

$$\mathbf{f}(\mathbf{x}, t) = \int \mathbf{F}(\mathbf{s}, t)\delta(\mathbf{x} - \mathbf{X}(\mathbf{s}, t))d\mathbf{s}, \tag{22}$$

where $\mathbf{f}(\mathbf{x}, t)$ is the fluid body force density and δ is a smoothed approximation of the Dirac Delta function. In the present 3D study, the function is chosen to be

$$\delta(\mathbf{x} - \mathbf{X}(\mathbf{s}, t)) = \delta(x - X(\mathbf{s}, t))\delta(y - Y(\mathbf{s}, t))\delta(z - Z(\mathbf{s}, t)), \tag{23}$$

where

$$\delta(r) = \begin{cases} \frac{1}{4}\left(1 + cos\left(\frac{\pi|r|}{2}\right)\right), & r \le 2 \\ 0, & r > 2. \end{cases} \tag{24}$$

The same approximation function is used to obtain the velocities of the Lagrangian nodes on the moving boundary. The mathematical form can be written as follows:

$$\frac{\partial \mathbf{X}}{\partial t} = \int \mathbf{u}(\mathbf{x}, t)\delta(\mathbf{x} - \mathbf{X}(\mathbf{s}, t))d\mathbf{x}. \tag{25}$$

To take into account the fluid body force density $\mathbf{f}(\mathbf{x}, t)$, an extra term $F_i\Delta t$ should be added into the right hand side of the LBE (Eq. (16)) [40], i.e.,

$$F_i\Delta t = (1 - \frac{1}{2\tau})\Delta t\omega_i\left[\frac{\mathbf{e}_i - \mathbf{u}}{c_s^2} + \frac{(\mathbf{e}_i \cdot \mathbf{u})}{c_s^4}\mathbf{e}_i\right] \cdot \mathbf{f}. \tag{26}$$

Correspondingly, the equation for momentum of the fluid, i.e., Eq. (20), should be replaced by

$$\rho\mathbf{u} = \sum_i f_i\mathbf{e}_i + \frac{1}{2}\mathbf{f}\Delta t. \tag{27}$$

The validations of this method, such as the grid-independence and time step-independence studies, and deformation of capsule in simple shear flow, have been presented in details in [16,34]. Here, the computational domain is a cubic box with side $10R_0$ which is large enough to neglect the boundary effect. The grid resolutions in the fine and coarse blocks are $\Delta x_f = \Delta y_f = \Delta z_f = R_0/12$ and $\Delta x_c = \Delta y_c = \Delta z_c = R_0/6$, respectively.

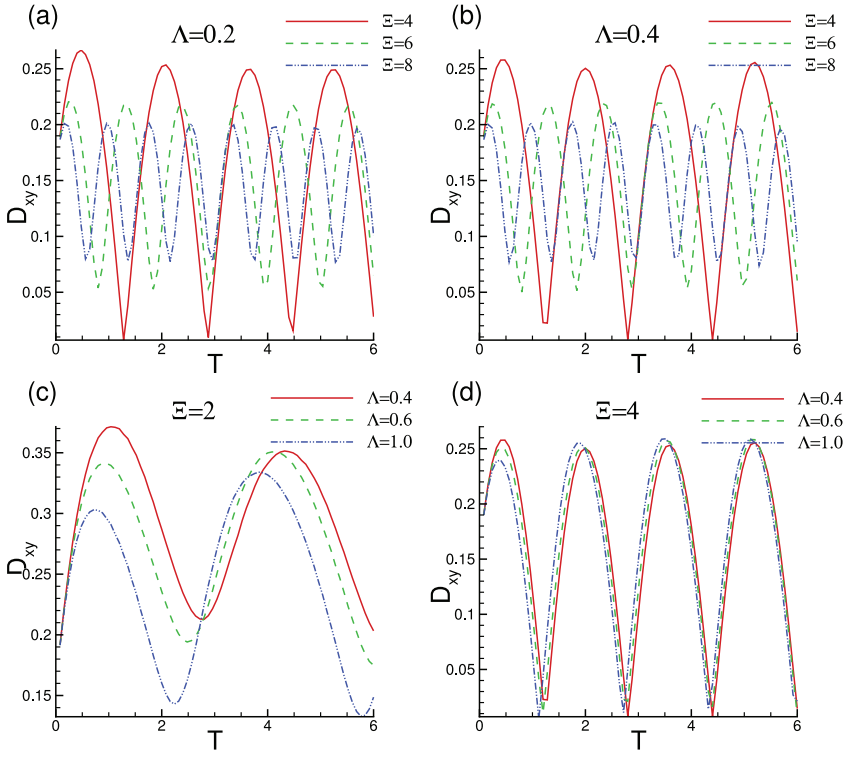

Fig. 3. The evolution of the capsule. (a) $\Lambda = 0.2$ and (b) $\Lambda = 0.4$ with different Ξ; (c) $\Xi = 2$ and (d) $\Xi = 4$ with different Λ.

The initial velocity field is prescribed by Eq. (3). The velocity distribution on the boundaries is fixed as that in the initial state (Eq. (3)). Since the velocities on the boundary nodes are specified, the velocity boundary condition proposed by Zou and He [41] can be implemented for each boundary nodes. Due to the low Reynolds flow ($Re \approx 0.01$) and small size of the capsule compared to the whole computational domain, the perturbation of the capsule on the flow is very small and the fixed velocity boundary condition is valid.

The capsule is discretized into 8192 triangular elements connecting 4098 nodes. The capsule is initially oblate with shape parameter $r_2 = \frac{a_2}{a_1} = \frac{10}{11}$ unless it is specially stated, the initial inclination angle is $\frac{\pi}{4}$. The Taylor deformation parameter D_{xy} is

$$D_{xy} = \frac{L - B}{L + B}, \tag{28}$$

where L and B are semi-major and semi-minor axes, respectively. The time is nondimensionalized by $\frac{1}{2s}$.

3. Results and discussion

3.1. Shape dynamics of a capsule in general flow

It is noted that in our derivation, i.e., Eq. (11), the shape of the capsule is supposed to be fixed. However, the shape will change continuously in the numerical simulation. Hence, the numerical results will be different from the theoretical results. In the follows, effects of the two dimensionless parameters Ξ and Λ on the deformation of the capsule are studied numerically in detail.

Usually Λ dominates the deformation of the capsule because Λ is the ratio of elastic stress to viscous force of the fluid exerting on the capsule. However, from Fig. 3(a) and (b), it is seen that Ξ also affect the capsule deformation and for a fixed Λ, the deformation of capsule decreases with the increase of Ξ, which is similar to the effect of viscosity ratio λ on the capsule deformation [10]. It is also found that a larger Ξ results in a shorter period of the deformation.

The effect of Ξ is similar to that of λ but with some differences. In the effect of λ, increasing λ makes the capsule more viscous and the dynamic force in the membrane increases even the strain rate s is fixed. However, the increasing of Ξ results in the acceleration of the rotation of the flow and it can not change the dynamic force if the strain rate s is fixed [24]. Because the deformation of the capsule would need time to evolve, when Ξ is larger, the evolution period is reduced and the deformation magnitude is suppressed. That is shown in Fig. 3(a) and (b).

The period of the deformation is mainly determined by Ξ. Through many tests with different Λ and Ξ, it is found that the period of deformation T_D times Ξ is a constant, i.e.,

$$T_D \Xi = 1/C_0, \tag{29}$$

where $C_0 = 0.15625$. Hence, $2\pi/(\Xi T_D) = 2\pi C_0 = 1$. This is also supported by cases of $\Xi = 4$ and $\Xi = 8$ in Fig. 3(a) and (b). It is seen that the period in the case of $\Xi = 4$ is two times of that in the case $\Xi = 8$.

From Fig. 3(c), it is seen that when Ξ is relatively small, the deformation magnitude decreases with the increase of Λ. However, from Fig. 3(d), we can see that when Ξ is large, the deformation is almost independent of Λ. As the explanation mentioned above, if Ξ is large enough, capsule would experience the same deforming procedure no matter what Λ is. In other words, as T_D is inversely proportional to Ξ, if Ξ is large enough to suppress the deformation procedure of the case with the largest Λ (e.g., $\Lambda = 1.0$ in Fig. 3(d)), then all of the cases with other smaller Λ would undergo the same suppressed procedure.

We give a brief theoretical explanation to the influence of Ξ on the deformation of the capsule. Here, following [27], we only consider a nearly spherical capsule, the radial position r_s of the surface of the capsule membrane can be expressed by

$$r_s = 1 + \varepsilon f(\vartheta, \varphi, t), \tag{30}$$

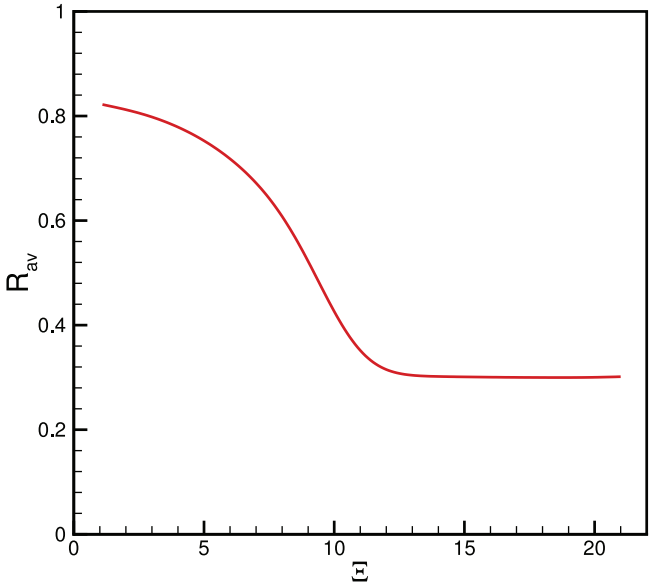

Fig. 4. The average value of R over one period as a function of Ξ when $\Lambda = 0.2$.

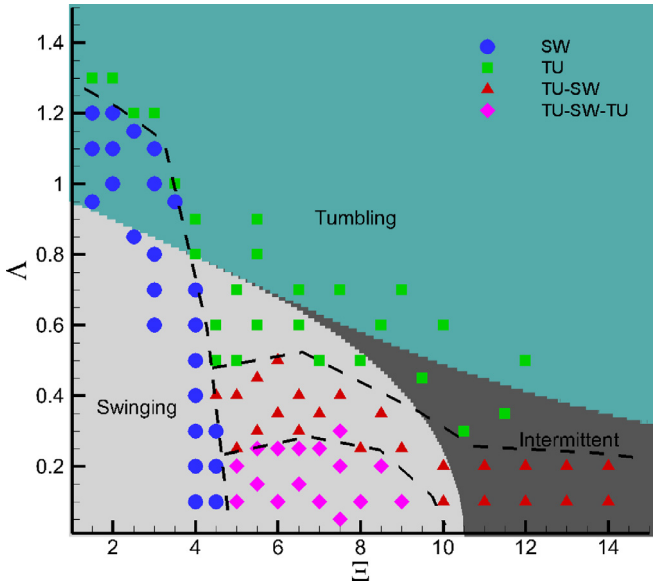

Fig. 5. Phase diagram of the capsule dynamical states in general flow. The grey scales represent the three regimes obtained by theoretical model. The symbols and the dashed lines represent numerical results. Blue filled circles, green filled squares, and red filled triangles represent SW, TU, and TU-SW transition modes, respectively. Pink filled diamonds denote TU-SW-TU mode. The dashed lines represent boundaries of different modes. (For interpretation of the references to color in this figure legend, the reader is referred to the web version of this article.)

where f is the deviation of the capsule shape from a spherical shape. f is expanded into series of scalar spherical harmonics Y_{jm},

$$f = \sum_{j=2}^{\infty} \sum_{m=-j}^{j} f_{jm} Y_{jm}. \tag{31}$$

We add the rotational part of the flow to the governing Eq.(3.16) in [27], then it can be written as

$$\frac{\partial f_{22}}{\partial T} = i\Xi f_{22} - i\Gamma - \Pi(f_{22} - g_{22}), \tag{32}$$

where $\Gamma = \frac{8\sqrt{30\pi}}{(23\lambda+32)\sqrt{\Delta}}$, $\Pi = \frac{16E}{6(23\lambda+32)\mu s R_0}$ and g_{22} is the initial shape function with the same definition of f_{22}. If we set

$$f_{22} = Rexp(-2i\theta), \tag{33}$$

where R is a parameter connected with the Taylor deformation parameter D_{xy} (see Eq. (35)), we can obtain the shape evolution equation

$$\frac{\partial R}{\partial T} = \Gamma sin2\theta - \Pi R + \frac{1}{2}\Pi\sqrt{\Delta} cos(2\phi - 2\theta). \tag{34}$$

We use the result of Eq. (11) to obtain the value of θ and ϕ, then the shape equation is solved by Runge–Kutta scheme. The average value of R as a function of Ξ is shown in Fig. 4 with $\Lambda = 0.2$.

The Taylor deformation parameter can also been written as a function of R [42]

$$D_{xy} \approx \frac{R}{8}\sqrt{\frac{15\Delta}{\pi}}. \tag{35}$$

From Fig. 4, we can see R decreases with the increase of Ξ when Ξ is not large, which means that increasing Ξ suppresses the deformation of the capsule. In Eq. (11), the capsule is assumed to be a shape-preserving ellipsoid. Usually, theoretical studies have to adopt this assumption to simplify the analysis. Although there is a discrepancy between the assumption and the reality, Eq. (11) provides the theoretical basis for further analysis. If the deformation of the capsule is considered at beginning, the governing equations for the motion of the capsule would be very complicated. Here after the theoretical results from Eq. (11) are obtained, Eq. (34) is adopted, which includes the effect of deformation. In this way, we got preliminary solution taking into account the deformation effect. Then we are able to explain the numerical results qualitatively.

3.2. Intermittent dynamics

The normalized mean tumbling rate is defined as [24,42]

$$\langle\dot{\theta}\rangle \equiv \frac{\langle\partial_T\theta\rangle}{\langle\partial_T\theta\rangle + \langle\partial_T\phi\rangle}, \tag{36}$$

where

$$\langle\partial_T\theta\rangle \equiv \lim_{t\to\infty}\frac{1}{t}\int_0^t \partial_T\theta(T)dT,$$
$$\langle\partial_T\phi\rangle \equiv \lim_{t\to\infty}\frac{1}{t}\int_0^t \partial_T\phi(T)dT. \tag{37}$$

In a pure tumbling motion, the inclination angle θ grows continuously while the phase angle ϕ oscillates, which implies the mean tumbling rate $\langle\dot{\theta}\rangle = 1$ for a large time t. On the contrary, in a pure swinging motion, the phase angle ϕ grows without bounds while the inclination angle θ oscillates, which implies $\langle\dot{\theta}\rangle = 0$ for a large t. Obviously, the intermittent regime corresponds to a mean tumbling rate between 0 and 1.

Here, different dynamic modes are identified according to the evolution of inclination angle in our numerical study. The phase diagram of different regimes spanning on the (Ξ, Λ) plane is shown in Fig. 5. Three grey scale regimes represent SW, Intermittent, TU modes, which are obtained through solving Eq. (11) by fourth order Runge–Kutta scheme. Here, Eq. (34) is not used. If the shape deformation is taken into account, i.e., incorporating Eq. (34) into Eq. (11), Eq. (11) would be very difficult to solve because the coefficients in Eq. (11), such as h_1, h_2 and h_3 are all functions of time. For example, the coefficients in h_1 will be very complicated (see (A.8) and (A.10)).

The numerical simulation results are also shown in Fig. 5. The symbols and the dashed lines are the modes and boundaries of different modes, respectively. Blue filled circles, green filled squares, and red filled triangles represent SW, TU, and TU-SW transition modes, respectively. Pink filled diamonds denote the new mode that we find: TU-SW-TU mode. It is seen that the boundaries predicted theoretically are not consistent with those obtained from

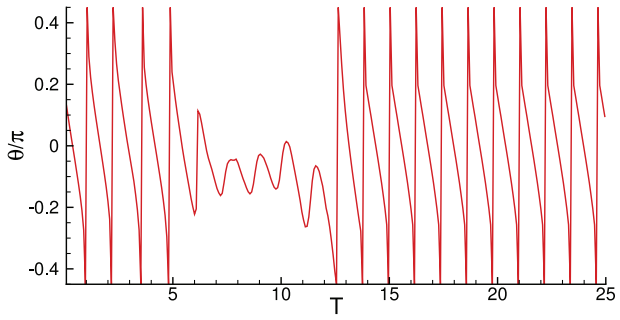

Fig. 6. The evolution of inclination angle with $\Xi = 5, \Lambda = 0.1$.

the numerical results. However, it is not surprise because in the present theoretical predictions, the capsule shape is initially fixed. The theoretical predictions will be close to the numerical results if the initial shape is replaced by the deformed shape in the theoretical model [24,42]. Because the shape deformation as a function of time depends on not only Λ but also Ξ, it would be difficult to theoretically analyze the deformation [25,26].

From the Fig. 5 we see that the profile of the distribution of the modes is similar to the results of [42], in which the horizontal axis is the viscosity ratio. Here we present some connections between the viscosity ratio λ and dimensionless parameter Ξ. If Eq. (11) is divided by $-h_1 = \frac{1}{\lambda^*}$, it yields

$$\begin{aligned} \partial_\tau \phi &= -(\Lambda sin2\phi + cos2\theta), \\ \partial_\tau \theta &= -\frac{1}{2}\Xi\lambda^* - h_2\partial_\tau\phi + h_3\lambda^* cos2\theta, \end{aligned} \tag{38}$$

where $\tau = T/\lambda^*$. if we set $\Xi = 1$, it would reduce to the expression in [42]. From Eq. (38), it is seen that there are two terms in the evolution equation of θ containing λ^*. However, there is only one term including the parameter Ξ. To analyze contributions of these two terms, first we assumed that $\Xi\lambda^*$ is a constant. If λ^* is small and Ξ is large, then contribution of the third term in the RHS of the second equation in Eq. (38) is minor compared to the first term. Under this circumstance, the two cases that only changing λ^* and only changing Ξ contribute equivalently to the equation. Hence, in the region of large Ξ, the phase (mode) distributions in the phase diagram that we obtained (see Fig. 5) is consistent with those in the literature [3,23,24].

If λ^* is large ($\Xi\lambda^* = const$), then contribution of the last term in the RHS of Eq. (38) is comparable to the first term. The two cases that only changing λ^* and only changing Ξ are different, then it would lead to different results for the evolution of θ. In this situation, Ξ is not large enough, the phase distribution in the phase diagram is different from those in previous studies, which is discussed following.

Here we focus on the new transition mode of TU-SW-TU, which is shown in Fig. 6 with the parameters $\Xi = 5, \Lambda = 0.1$. In the transition mode, an initially tumbling mode transfers to swinging mode, and then it would return to a tumbling mode, and within our simulation time ($T = 40$) it will maintain this steady tumbling mode. In [3] and [23], the transition is always one way, in which the capsule would maintain a stable swinging mode after transition from tumbling, and this cannot reverse. Fig. 6 shows that the SW motion continues for about 8 dimensionless time (approximately $5 \le T \le 13$). The SW may be not transient because the capsule has sufficient time to adapt with the imposed flow. According to previous studies, the SW motion is more stable than tumbling (TU) motion. That is why only one way transition (TU-SW) is observed in the literature. Recently, Cordasco et al. [4] proposed a mechanism that the membrane in-plane elastic energy is relevant to the intermittent motion of RBC. However, here the capsule is an ellipsoid particle which is different from the RBC with circular biconcave discoid shape, such mechanism does not work.

Now we provide an explanation for the observed dynamics in numerical simulations. As shown in Fig. 5, the region of the TU-SW-TU transition is constricted to a range with a moderate Ξ and low Λ. The energy barrier theory reveals that the capsule with lower Λ would be more likely to overcome the energy barrier due to large hydrodynamic shear force. However, the conclusion is based on the assumption that the deformation is large when the capsule has a lower Λ. Here, the deformation is small at a lower Λ. As discussed in Sec. 3.1, large Ξ would confine the deformation, which implies that the deformation along vorticity direction is constant or changing little due to volume preservation. That is consistent with the explanation of [27]. In other words, at this range (approximately $5 < \Xi < 10$, and low Λ), the effect of constraint on the deformation along vorticity direction is dominated, which is totally different from the energy barrier mechanism.

When Ξ is moderate (approximately $\Xi \approx 6$), the capsule with smaller Λ deforms less than that in the cases of $\Xi = 1$, which is a purely shear flow, i.e., due to the rotation of the fluid, the suppression to the deformation is stronger. So, the capsule with small Λ is more likely to transit to tumbling mode than the capsules with large Λ. While when Ξ becomes larger, the deformations are almost identical and independent of Λ. Under this circumstance, the deformation would not affect the transition. On the condition, the energy barrier theory is valid, in which when Λ is low, the fluid shear stress acting on the capsule is sufficient to force the membrane to tank tread [9].

In present work, our object is capsule, a kind of membrane which provides shear resistance without bending effect. On the other hand, the bending resistance may not alter the TB-SW-TB transition. Cordasco et al. [4] studied the motion of red blood cell dynamics using the model with shear and bending effect. At page 484 in [4], Cordasco et al. pointed out that the intermittent motion is relevant to the in-plane energy and the bending resistance has little effect on the transition boundary. So, here we did not consider the effect of bending.

3.3. Effects of initial aspect ratio and initial inclined angle

In simple shear flow, the effect of initial aspect ratio has been studied in [10,15] and it has been found that a capsule deviating largely from spherical profile is more likely to transit to tumbling mode. Fig. 7 shows the aspect ratio effect on the transition dynamics in our study. From Fig. 7, it is seen that in the simple shear flow ($\Xi = 1$), capsules with small initial aspect ratio could transit to tumbling motion with softer membrane (lower Λ), which is consistent with that observed in [10,15]. Actually not only $\Xi = 1$ but also the other $\Xi > 1$, the similar situation can be observed, i.e., for cases with smaller initial aspect ratio, transition to tumbling motion becomes easier (with lower Λ) (see Fig. 7).

From Fig. 7, it is also seen that for the same Λ, a capsule with smaller initial aspect ratio would transit to tumbling motion at a lower Ξ. Here Ξ represents the rotational strength of the fluid. Hence, the capsule needs less rotation effect of the fluid to transit to tumbling mode. For the TU-SW and TU-SW-TU transition modes, the situation is similar, i.e., less rotation effect (lower Ξ) is required for cases with smaller initial aspect ratio. Hence, the boundaries between different modes are all shifted to lower Ξ and Λ regime for the capsule with smaller initial aspect ratio.

The effect of the initial inclined angle on the TU-SW-TU is also investigated. The phase diagrams for different initial angles ($\theta_0 = 0, \frac{\pi}{8}, \frac{3\pi}{8}, \frac{4\pi}{8},$) are all similar with negligible discrepancies (not shown). Hence, the initial inclined angle almost has no effect on the mode transition.

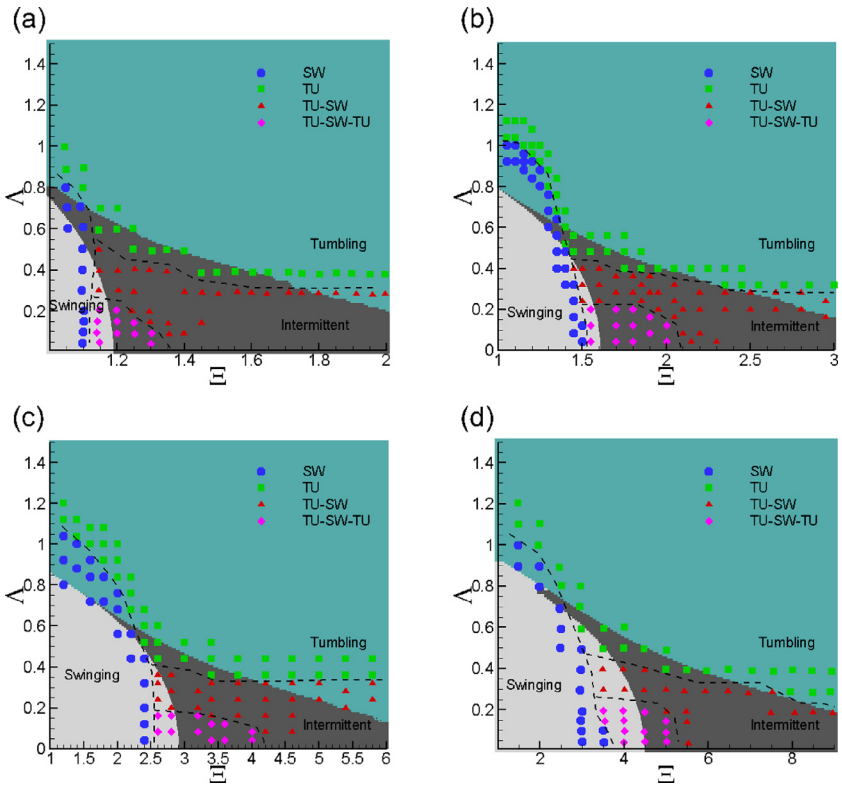

Fig. 7. Phase diagrams for capsule dynamic states with different initial aspect ratio. (a) $r_2 = 0.3$, (b) $r_2 = 0.5$, (c) $r_2 = 0.7$ and (d) $r_2 = 0.8$. Note that the horizontal axis ranges are different in each plot.

3.4. Rheology of dilute suspension

Instead of the dimensionless particle stress tensor [2,43], here the intrinsic viscosity [35,44] is used to evaluate the contribution of the capsules on the bulk rheology.

$$[\eta] = \frac{\eta_{eff} - 1}{\Omega}, \tag{39}$$

where η_{eff} is the dimensionless effective viscosity defined as $\eta_{eff} = \frac{\tilde{\sigma}_{12}}{2e^0_{12}}$, and Ω is the concentration. Substituting Eq. (A.2) into Eq. (39), the intrinsic viscosity can be calculated as

$$\begin{aligned}[\eta] &= \frac{\mu A^*_{12}}{2e^0_{12}\Omega} = \frac{4\mu}{\Omega}\frac{g_1 e^*_{12} - \alpha_2^2 g_3^{'}\left(\zeta^*_{12} - \varepsilon_{12k}\dot{\theta}\right)}{g_3^{'}\left(\alpha_1^2 g_1 + \alpha_2^2 g_2\right)}\frac{1}{2scos(2\theta)} \\ &= \frac{4\mu}{\Omega}\frac{1}{J}\{M - N(\Lambda sin2\phi + cos2\theta)\},\end{aligned} \tag{40}$$

where $J = g_3^{'}(\alpha_1^2 g_1 + \alpha_2^2 g_2)$, $M = \frac{1}{2}g_1 + \alpha_2^2 g_3^{'} h_3$ and if we set $tan\alpha = \frac{a_1^2 - a_2^2}{2a_1 a_2}$, then $N = h_1(g_1 tan\alpha + \frac{\alpha_2^2 g_3^{'}}{cos\alpha} - h_2\alpha_2^2 g_3^{'})$. It seems that Eq. (8) does not contain the parameter Ξ, which means that the rotation of the fluid flow has no contribution to the bulk rheology of the flow.

However, Ξ plays an important role in the rheology of the suspension through the shape dynamics effect because J, M and N are all functions of shape parameters. Hence, they should be functions of Ξ. This result of a dilute suspension ($\Omega \ll 1$) is shown in Fig. 8. The mean value of intrinsic viscosity, $[\bar{\eta}]$, is computed by averaging $[\eta]$ over one period. It is seen that for a specific Ξ, $[\bar{\eta}]$ increases with Λ.

It is also found that $[\bar{\eta}]$ decreases with Ξ for the same Λ. Here, for a given Λ, a larger Ξ could shorten the period of the disturbance of the capsule on the flow, i.e., the Ξ suppresses the disturbance. Gao et al. [35] proposed that if the particles in the suspension disturb the flow less, the intrinsic viscosity may decrease. Hence, $[\bar{\eta}]$ would become smaller. It is also seen from Fig. 8 that $[\bar{\eta}]$ may be less than 0, which indicates that the suspension is less viscous than the fluid in some special conditions [35].

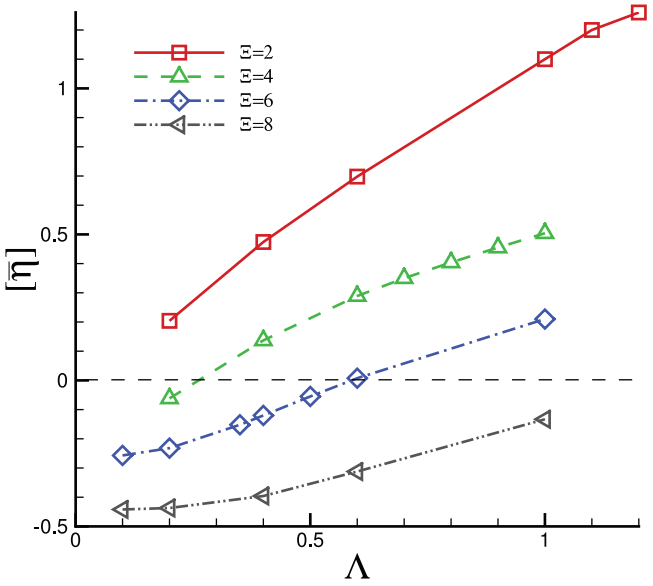

Fig. 8. The mean intrinsic viscosity $[\bar{\eta}]$ as a function of Λ for cases $\Xi = 2, 4, 6, 8$.

4. Conclusion

We have investigated the dynamics of a nonspherical capsule in general flow using theoretical and numerical analyses. The numerical results have discrepancies with the theoretical results due

to the fixed shape assumption in the theoretical analysis. On the other hand, we focus on analyzing the transition dynamics. Two transition behaviors (the TU-SW transition and TU-SW-TU transition) are found in the intermittent regime, which is different from the intermittent behavior predicted by theoretical models. To the best of our knowledge, the TU-SW-TU transition has not been observed in capsule dynamics up to now and it is the first time that we obtained this transition in general flow. The mechanism for the TU-SW-TU transition may be associated with the deformation along the vorticity direction. The effects of Ξ (the ratio of vorticity to the strain rate) on the deformation of capsule is demonstrated. It seems that Ξ suppresses the deformation in the vorticity direction, which triggers the TU-SW-TU transition. Also, the effect of initially aspect ratio of the capsule is investigated. The result shows that a capsule deviating largely from spherical profile is more likely to transit to tumbling mode, which is similar to the situation of a capsule in simple shear flow. Finally, the intrinsic viscosity as functions of the two dimensionless parameters Λ and Ξ is studied by theoretical and numerical analyses.

Acknowledgments

Huang is supported by National Natural Science Foundation of China (Grant No. 11172297), Anhui Provincial Natural Science Foundation(Grant No. 130808 5MA06), Program for New Century Excellent Talents in University,Ministry of Education, China (NCET-12-0506) and the Fundamental Research Funds for the Central Universities.

Appendix A. Stress field of the system

The velocity field of the membrane in the body-fixed frame is assumed to be

$$u_1^m = \nu_0(-a_1/a_2)x_2,\ u_2^m = \nu_0(a_2/a_1)x_1,\ u_3^m = 0, \tag{A.1}$$

where ν_0 is defined as $\nu_0 = \partial\phi/\partial t$. ϕ is phase angle shown in Fig. 1. Then the stress tensor can be written as

$$\sigma_{ij} = -p\delta_{ij} + \mu(A_{ij}^* + 2e_{ij}^m), \tag{A.2}$$

where p is an arbitrary constant pressure and e_{ij}^m is defined as

$$e_{ij}^m = \frac{1}{2}(u_{j,i}^m + u_{i,j}^m). \tag{A.3}$$

The tensor A_{ij}^* are independent of x_i, two elements of A_{ij}^* are

$$\begin{cases} A_{11}^* = \dfrac{4}{3}\dfrac{2g_1e_{11}^* - g_2e_{22}^* - g_3e_{33}^*}{g_2''g_3'' + g_3''g_1'' + g_1''g_2''}, \\ A_{12}^* = 4\dfrac{g_1e_{12}^* - \alpha_2^2g_3'(\zeta_{12}^* - \epsilon_{123}\dot{\theta})}{g_3'(\alpha_1^2g_1 + \alpha_2^2g_2)}, \end{cases} \tag{A.4}$$

where

$$e_{ij}^* = e_{ij}^0 - e_{ij}^m, \tag{A.5}$$

$$e_{ij}^0 = \frac{1}{2}(u_{j,i}^0 + u_{i,j}^0), \tag{A.6}$$

and

$$\begin{cases} \zeta_{ij}^* = \zeta_{ij}^0 - \zeta_{ij}^m, \\ \zeta_{ij}^0 = \dfrac{1}{2}(u_{j,i}^0 - u_{i,j}^0), \\ \zeta_{ij}^m = \dfrac{1}{2}(u_{j,i}^m - u_{i,j}^m). \end{cases} \tag{A.7}$$

The other parameters are

$$\begin{cases} g_1 = \int_0^\infty \dfrac{ds}{(\alpha_1^2+s)\Delta}, \\ g_1' = \int_0^\infty \dfrac{ds}{(\alpha_2^2+s)(\alpha_3^2+s)\Delta}, \\ g_1'' = \int_0^\infty \dfrac{sds}{(\alpha_2^2+s)(\alpha_3^2+s)\Delta}, \\ \Delta^2 = (\alpha_1^2+s)(\alpha_2^2+s)(\alpha_3^2+s), \end{cases} \tag{A.8}$$

where α_i denotes the dimensionless axes

$$\alpha_i = a_i/a_0, \tag{A.9}$$

and $a_0 = (a_1a_2a_3)^{\frac{1}{3}}$. $\dot{\theta}$ is the angular velocity of the ellipsoid in the space-fixed frame. The other elements of A_{ij}^* and the integrals $g_2, g_2'...$ could be obtained by the permutation of the subscripts.

The parameters in (5) and (6) are defined as:

$$\begin{aligned} &r_2 = a_2/a_1,\ r_3 = a_3/a_1, \\ &z_1 = \frac{1}{2}(r_2^{-1} - r_2),\ z_2 = g_3'(\alpha_1^2 + \alpha_2^2), \\ &f_1 = (r_2 - r_2^{-1})^2,\ f_2 = 4z_1^2(1 - 2/z_2),\ f_3 = -4z_1/z_2, \end{aligned} \tag{A.10}$$

Appendix B. The elastic energy form for capsule

According to the theoretical model, the element on the membrane is assumed to move along a ellipsoidal shape, then the kinematic equation of membrane can be described by [10]

$$\begin{aligned} x_1 &= x_1^0 cos\phi - \frac{1}{r_2}x_2^0 sin\phi, \\ x_2 &= x_2^0 cos\phi + r_2x_1^0 sin\phi, \\ x_3 &= x_3^0, \end{aligned} \tag{B.1}$$

where x_i^0 defines the initial position of a material point in the membrane at time $t = 0$. Hence the deformation gradient tensor is

$$F_{ij} = \begin{bmatrix} cos\phi & -\dfrac{sin\phi}{r_2} & 0 \\ r_2 sin\phi & cos\phi & 0 \\ 0 & 0 & 1 \end{bmatrix}. \tag{B.2}$$

The left Cauchy-Green tensor is

$$\begin{aligned} V^2 &= F \cdot F^T \\ &= \begin{bmatrix} cos^2\phi + \dfrac{sin^2\phi}{r_2^2} & r_2 sin\phi cos\phi - \dfrac{1}{r_2}sin\phi cos\phi & 0 \\ r_2 sin\phi cos\phi - \dfrac{1}{r_2}sin\phi cos\phi & r_2^2 sin^2\phi + cos^2\phi & 0 \\ 0 & 0 & 1 \end{bmatrix}. \end{aligned} \tag{B.3}$$

Then we set $det\left|V^2\right| = 0$,

$$\begin{aligned} &\underline{\lambda}^2 - \left(2cos^2\phi + \frac{sin^2\phi}{r_2^2} + r_2^2 sin^2\phi\right)\underline{\lambda} + \left(cos^2\phi + \frac{sin^2\phi}{r_2^2}\right) \\ &\times (r_2^2 sin^2\phi + cos^2\phi) - 4z_1 sin^2\phi cos^2\phi = 0. \end{aligned} \tag{B.4}$$

It yields

$$\begin{aligned} \lambda_1^2 + \lambda_2^2 &= r_2^2 sin^2\phi + \frac{sin^2\phi}{r_2^2} + 2cos^2\phi \\ &= \left(r_2^2 + \frac{1}{r_2^2} - 2\right)sin^2\phi + 2 \\ &= 4z_1^2 sin^2\phi + 2, \end{aligned} \tag{B.5}$$

$$\lambda_1^2\lambda_2^2 = \left(cos^2\phi + \frac{sin^2\phi}{r_2^2}\right)(r_2^2 sin^2\phi + cos^2\phi) - 4z_1 sin^2\phi = 1. \quad \text{(B.6)}$$

The first and second strain invariants I_1 and I_2 are

$$I_1 = \lambda_1^2 + \lambda_2^2 - 2 = 4z_1^2 sin^2\phi,$$
$$I_2 = \lambda^2\lambda^2 - 1 = 0. \quad \text{(B.7)}$$

For the neo-Hookean Law [17,34], we have

$$W^{NH} = \frac{1}{6}E\left(I_1 - 1 + \frac{1}{I_2 + 1}\right) = \frac{1}{6}EI_1 = \frac{2}{3}z_1^2 E sin^2\phi. \quad \text{(B.8)}$$

References

[1] Abkarian M, Faivre M, Viallat A. Swinging of red blood cells under shear flow. Phys Rev Lett 2007;98(18):188302.
[2] Bagchi P, Kalluri RM. Dynamic rheology of a dilute suspension of elastic capsules: effect of capsule tank-treading, swinging and tumbling. J Fluid Mech 2011;669:498–526.
[3] Kessler S, Finken R, Seifert U. Swinging and tumbling of elastic capsules in shear flow. J Fluid Mech 2008;605:207–26.
[4] Cordasco D, Bagchi P. Intermittency and synchronized motion of red blood cell dynamics in shear flow. J Fluid Mech 2014;759:472–88.
[5] de Loubens C, Deschamps J, Boedec G, Leonetti M. Stretching of capsules in an elongation flow, a route to constitutive law. J Fluid Mech 2015;767:R3.
[6] Sui Y, Chen X, Chew Y, Roy P, Low H. Numerical simulation of capsule deformation in simple shear flow. Comput Fluids 2010a;39(2):242–50.
[7] Sui Y, Low H, Chew Y, Roy P. A front-tracking lattice boltzmann method to study flow-induced deformation of three-dimensional capsules. Comput Fluids 2010b;39(3):499–511.
[8] Ye H, Huang H, Lu X-Y. Numerical study on dynamic sorting of a compliant capsule with a thin shell. Comput Fluids 2015;114:110–20.
[9] Skotheim J, Secomb T. Red blood cells and other nonspherical capsules in shear flow: oscillatory dynamics and the tank-treading-to-tumbling transition. Phys Rev Lett 2007;98(7):078301.
[10] Keller SR, Skalak R. Motion of a tank-treading ellipsoidal particle in a shear flow. J Fluid Mech 1982;120:27–47.
[11] Barthes-Biesel D. Motion of a spherical microcapsule freely suspended in a linear shear flow. J Fluid Mech 1980;100(04):831–53.
[12] Barthes-Biesel D, Rallison J. The time-dependent deformation of a capsule freely suspended in a linear shear flow. J Fluid Mech 1981;113:251–67.
[13] Chang K, Olbricht W. Experimental studies of the deformation of a synthetic capsule in extensional flow. J Fluid Mech 1993;250:587–608.
[14] Ramanujan S, Pozrikidis C. Deformation of liquid capsules enclosed by elastic membranes in simple shear flow: large deformations and the effect of fluid viscosities. J Fluid Mech 1998;361:117–43.
[15] Wang Z, Sui Y, Spelt PD, Wang W. Three-dimensional dynamics of oblate and prolate capsules in shear flow. Phys Rev E 2013;88(5):053021.
[16] Sui Y, Chew Y, Roy P, Cheng Y, Low H. Dynamic motion of red blood cells in simple shear flow. Phys Fluids 2008a;20(11):112106.(1994-present)
[17] Gao T, Hu HH, Ponte Castañeda P. Dynamics and rheology of elastic particles in an extensional flow. J Fluid Mech 2013;715:573–96.
[18] Dupin MM, Halliday I, Care CM, Alboul L, Munn LL. Modeling the flow of dense suspensions of deformable particles in three dimensions. Phys Rev E 2007;75(6):066707.
[19] Finken R., Seifert U.. Wrinkling of microcapsules in shear flow. arXiv preprint cond-mat/06015892006.
[20] Walter A, Rehage H, Leonhard H. Shear induced deformation of microcapsules: shape oscillations and membrane folding. Colloid Surf A 2001;183:123–32.
[21] Barthès-Biesel D. Capsule motion in flow: deformation and membrane buckling. Comptes Rendus Physique 2009;10(8):764–74.
[22] Fischer TM. Shape memory of human red blood cells. Biophys J 2004;86(5):3304–13.
[23] Bagchi P, Kalluri RM. Dynamics of nonspherical capsules in shear flow. Phys Rev E 2009;80(1):016307.
[24] Finken R, Kessler S, Seifert U. Micro-capsules in shear flow. J Phys 2011;23(18):184113.
[25] Noguchi H. Dynamic modes of microcapsules in steady shear flow: effects of bending and shear elasticities. Phys Rev E 2010;81(5):056319.
[26] Noguchi H. Swinging and synchronized rotations of red blood cells in simple shear flow. Phys Rev E 2009;80(2):021902.
[27] Vlahovska P, Young Y-N, Danker G, Misbah C. Dynamics of a non-spherical microcapsule with incompressible interface in shear flow. J Fluid Mech 2011;678:221–47.
[28] Cordasco D, Yazdani A, Bagchi P. Comparison of erythrocyte dynamics in shear flow under different stress-free configurations. Phys Fluids 2014;26(4):041902.(1994-present)
[29] Peng Z, Mashayekh A, Zhu Q. Erythrocyte responses in low-shear-rate flows: effects of non-biconcave stress-free state in the cytoskeleton. J Fluid Mech 2014;742:96–118.
[30] Yazdani AZ, Bagchi P. Phase diagram and breathing dynamics of a single red blood cell and a biconcave capsule in dilute shear flow. Phys Rev E 2011;84(2):026314.
[31] Deschamps J, Kantsler V, Segre E, Steinberg V. Dynamics of a vesicle in general flow. Proc Nat Acad Sciences 2009;106(28):11444–7.
[32] Jeffery GB. The motion of ellipsoidal particles immersed in a viscous fluid. Proc R Soc London A 1922;102:161–79.
[33] Roscoe R. On the rheology of a suspension of viscoelastic spheres in a viscous liquid. J Fluid Mech 1967;28(02):273–93.
[34] Sui Y, Chew Y-T, Roy P, Low H-T. A hybrid method to study flow-induced deformation of three-dimensional capsules. J Comput Phys 2008b;227(12):6351–71.
[35] Gao T, Hu HH, Castañeda PP. Shape dynamics and rheology of soft elastic particles in a shear flow. Phys Rev Lett 2012;108(5):058302.
[36] Lebedev V, Turitsyn K, Vergeles S. Dynamics of nearly spherical vesicles in an external flow. Phys Rev Lett 2007;99(21):218101.
[37] Kaoui B, Farutin A, Misbah C. Vesicles under simple shear flow: Elucidating the role of relevant control parameters. Phys Rev E 2009;80(6):061905.
[38] Wang Z, Shi D, Zhang A. Three-dimensional lattice boltzmann simulation of bubble behavior in a flap-induced shear flow. Comput Fluids 2015;123:44–53.
[39] Yu D, Girimaji SS. Multi-block lattice boltzmann method: extension to 3d and validation in turbulence. Physica A 2006;362(1):118–24.
[40] Guo Z, Zheng C, Shi B. Discrete lattice effects on the forcing term in the lattice boltzmann method. Phys Rev E 2002;65(4):046308.
[41] Zou Q, He X. On pressure and velocity boundary conditions for the lattice boltzmann bgk model. Phys Fluids 1997;9(6):1591–8.(1994-present)
[42] Kessler S, Finken R, Seifert U. Elastic capsules in shear flow: analytical solutions for constant and time-dependent shear rates. Eur Phys J E: 2009;29(4):399–413.
[43] Batchelor G. The stress system in a suspension of force-free particles. J Fluid Mech 1970;41(03):545–70.
[44] Huang H, Yang X, Krafczyk M, Lu X-Y. Rotation of spheroidal particles in couette flows. J Fluid Mech 2012;692:369–94.